



HAL
open science

Late Quaternary environmental changes of Lake Urmia basin (NW Iran) inferred from sedimentological and magnetic records.

Alina Tudryn, Seyed-Hani Motavalli-Anbaran, Piotr Tucholka, E. Gibert, Mohammad Lankarani, Hesam Ahmady-Birgani, Ting Kong, Aurélie Noret, Serge Miska, Marc Massault, et al.

► To cite this version:

Alina Tudryn, Seyed-Hani Motavalli-Anbaran, Piotr Tucholka, E. Gibert, Mohammad Lankarani, et al.. Late Quaternary environmental changes of Lake Urmia basin (NW Iran) inferred from sedimentological and magnetic records.. Quaternary International, 2021, 589, pp.83-94. 10.1016/j.quaint.2021.03.024 . hal-03454996

HAL Id: hal-03454996

<https://hal.science/hal-03454996>

Submitted on 29 Nov 2021

HAL is a multi-disciplinary open access archive for the deposit and dissemination of scientific research documents, whether they are published or not. The documents may come from teaching and research institutions in France or abroad, or from public or private research centers.

L'archive ouverte pluridisciplinaire **HAL**, est destinée au dépôt et à la diffusion de documents scientifiques de niveau recherche, publiés ou non, émanant des établissements d'enseignement et de recherche français ou étrangers, des laboratoires publics ou privés.

1 **Late Quaternary environmental changes of Lake Urmia basin (NW Iran) inferred from**
2 **sedimentological and magnetic records**

3
4 Alina Tudryn^{1,*}, Seyed-Hani Motavalli-Anbaran², Piotr Tucholka¹, Elisabeth Gibert-Brunet¹,
5 Mohammad Lankarani³, Hesam Ahmady-Birgani⁴, Ting Kong¹, Aurélie Noret¹, Serge Miska¹,
6 Marc Massault¹, Olivier Dufaure¹

7 ¹University Paris-Saclay, CNRS, UMR 8148-GEOPS, 91405, Orsay, France

8 ²Institute of Geophysics, University of Tehran, Tehran, Iran

9 ³School of Geology, University-College of Science, University of Tehran, Tehran, Iran

10 ⁴Faculty of Natural Resources, Urmia University, Urmia, Iran

11
12 *Corresponding author

13 E-mail address: alina.tudryn@universite-paris-saclay.fr

14

15

16 Abstract

17 The ongoing changes affecting Lake Urmia (NW Iran) are revealed by the lake water level
18 decrease (~7 m in the last 20 yr) that was attributed to natural and anthropogenic causes but the
19 exact impact of these factors on the state of the lake is still not identified. Indeed, lack of detailed
20 record of environmental evolution of the lake in the past limits the understanding of actual and
21 future processes. Our project aims to obtain a high-temporal resolution record of environmental
22 changes in the lake area for the last ~30 kyrs. Sediment cores have been obtained from the
23 recently dried out part of the lake near Urmia City, and surface and ground waters have been
24 measured for electric conductivity. This paper presents results of water and sediments analyses.
25 Six ¹⁴C AMS dating on organic fractions provide a chronological framework and indicate that the
26 record covers the last ~30 cal kyr BP. During this period, evaporitic conditions were prevailing in
27 the lake. The electric conductivity of brines from the sediment highlights changes in the lake
28 water salinity. The data indicate a lake-level low stand at ~30 cal kyr BP that was followed by a
29 water level rise and establishment of lacustrine conditions for the next ~9 kyr, this phase
30 representing the highest lake level recorded since that time to date. From the LGM, the lake
31 experienced several fluctuations of the water level. The relatively long-term lacustrine condition
32 established during the Early Holocene before the water level decrease between ~5.5-4.9 cal kyr
33 BP. Sediments from the two dry events at ~30 cal kyr BP and at 5.5-4.9 cal kyr BP are
34 characterized by the presence of greigite, which indicates anaerobic early diagenetic conditions in
35 the sediment.

36

37 **Keywords:** Lake Urmia; Late Quaternary palaeoenvironments; Water level change; Carbonates;
38 Magnetic minerals; Electric conductivity

39 1. Introduction

40 Registered in the International Ramsar Convention and National Park in NW Iran, Lake Urmia
41 (Fig.1) is one of the largest saline lakes in the world displaying a unique, highly valuable
42 biodiversity (Asem et al., 2014). The lake plays a major role in creating the mild climate
43 favouring a highly productive agriculture and brine shrimp farming, both making the region as
44 one of the most important economical poles of Iran. However, since the end of the 1990's, Lake
45 Urmia's water level dropped drastically, and by more than 7 m during the last 20 years (Fig. 1b)
46 causing water hyper salinization, desertification and dust storms threatening health condition of
47 millions of people at a regional scale (Alipour, 2006; Pengra, 2012; Ahmady-Birgani et al., 2018;
48 2020). Although, subjected to controversies, the water level fall has been attributed to rainfall
49 declining by ~10% and to anthropogenic causes such as the construction of many dams on rivers
50 feeding the lake (Fig.1c) and intense groundwater pumping (Alipour, 2006; Pengra, 2012; Jalili et
51 al., 2016; Sharifi et al., 2018).

52 Despite evident water overexploitation, the role of natural *versus* anthropogenic factors
53 influencing the lake hydrology is still not quantified. The lack of detailed records of
54 environmental evolution in the past limits the understanding of actual processes and the capability
55 to develop integrated management of this water resource. As a matter of fact, the lake deposits
56 have not been extensively explored for palaeoenvironmental reconstructions. Already existing
57 sedimentological, geochemical and pollen studies of Pleistocene and Holocene sequences are
58 scarce. They cover large time scale (200 kyr) with a low resolution, generally missing the
59 Holocene (Djamali et al., 2008a, 2008b, 2010; Stevens et al., 2012) or focus on the Holocene with
60 a low temporal resolution (Kelts and Shahrabi, 1986; Bottema, 1986), or just concern its youngest
61 part (Talebi et al., 2015). However, all these studies show the highest amplitude lake-level
62 variations at a glacial-interglacial time scale with a dry open mountain steppe dominating during
63 the glacial periods and a steppe-forest environment during interglacials. An increase in tree
64 pollens during the Holocene was recorded at the transition from Early to Mid-Holocene, at 6.5 kyr

65 B.P., and similar to today's vegetation established. The vegetation reached its maximum
66 destruction due to increasing human impact during the last centuries. Saline deposition seems
67 almost continuous during the Holocene with clear water level changes but no visible total
68 desiccation of Lake Urmia.

69 The Franco-Iranian project initiated by bilateral Gundishapur program (2016-2017) on Lake
70 Urmia aims to obtain high temporal resolution records of past environmental and climate changes
71 in the SW lake area for the Late Pleistocene and Holocene, and to identify natural and human
72 impacts on the past hydro-environments of the lake and its catchment area. The process integrates
73 hydrogeological, hydrogeochemical and lake sediments studies. The obtained results will be
74 useful for the integrated approach of future Lake Urmia management and restoration of its
75 environment, and for studies of the past climate evolution at a larger, south Eurasian scale.

76 Indeed, the area is a place of choice being on the junction of the different air mass circulation
77 systems from the West (Atlantic, Mediterranean and North Sea) and from the East (Siberian and
78 Indian monsoon).

79 In this paper are presented the first results of water in-situ measurements (electric conductivity,
80 pH and temperature) and measurements on five collected sediment cores. The chronological
81 framework is based on six ^{14}C datings. The sedimentary sequence has been analysed for water
82 contents in sediment and corresponding relative salinity, grain size, magnetic minerals,
83 mineralogy of bulk sediment by X-Ray diffraction (XRD) and carbonate contents and
84 mineralogy. The goal of the study is (i) to provide the record of environmental changes in Lake
85 Urmia basin, mainly in terms of the lake water changes for the last ~30 cal kyr BP., (ii) to
86 complement the existing information on the evolution of the lake basin at the local scale and that
87 of the Middle East, and (iii) to contribute to a better understanding of relation between local
88 environment and the climate change.

89 **2. Setting**

90 *2.1 Lake Urmia*

91 Lake Urmia is an endorheic hypersaline lake located in a subsiding tectonic basin (Berberian and
92 Arshani, 1975) in NW Iran (Fig. 1). Before the recent water level fall, it was the largest lake in
93 the region after the Caspian Sea and the second largest salt lake on Earth, and presented similar in
94 physical, chemical and biological aspects to the Great Salt Lake in the USA (Kelts and Shahrabi,
95 1986). Lake Urmia was approximately 140 km long and 85 km wide, with a deeper northern
96 basin (maximal depth of ~16 m) and shallower southern one, salinity varying between 140 and
97 more than 220 g.L⁻¹ on an annual basis, a surface area of 5,000 to 6,000 km² and a catchment area
98 of approximately 52,500 km² (Sharifi et al., 2018). Although its salinity varied between 140 and
99 more than 220 g.L⁻¹ on an annual basis, the lake was geochemically homogeneous due to mixing
100 by strong water currents, particularly during spring (Alipour, 2006, Sharifi et al., 2018).
101 Nevertheless, Sharifi et al. (2018) show that in spring, the hydrochemistry of the southern part of
102 the lake at the vicinity of Simineh Rud and Zarrineh Rud river mouths (Fig. 1) becomes different
103 due to fresh water inflow to the lake, some stratification in water column was also observed
104 (report by Azarbaijan Regional Mining Cooperation, 1995). Lately, both basins were separated
105 by the Kalantari causeway, an east-west dike-type highway constructed in the 1980s – 1990s that
106 stretches on 15 km across the center of the lake with a gap of ~1.5 km on which a bridge was
107 constructed (1998-2008).

108 The lake basin is situated in a semi-arid zone. Prevailing winds are westerlies during winter,
109 northeasterlies during summer and strong southwesterlies during spring (Djamali et al., 2008a).
110 Today, the lake is supplied by direct precipitation (~300 mm.yr⁻¹), inflow from 13 permanent
111 rivers and also from periodic discharge into the lake by seasonal rivers and creeks (Alipour,
112 2006). According to Kelts and Shahrabi (1986), ancient terraces show evidence of large
113 fluctuations in lake level during Pleistocene. Historical documents and analysis of recent satellite
114 images show fluctuations ranging from 1.0 to 3.5 m, with an estimated lowest lake level during
115 the Little Ice Age (~XIV-XIX centuries; Kelts and Shahrabi, 1986; Alipour, 2006). Nevertheless,
116 from its highest level in the mid-1990s (1,278 m a.s.l.), the lake level has decreased by 7 m to

117 1,271 m a.s.l. in 2010, reducing the surface of the lake from 5700 km² to 4610 and after that to ~
118 2400 km² (Fig. 1b), resulting in the salinity increase above 300 g.L⁻¹ and dramatic ecologic
119 consequences for the lake catchment area (Alipour 2006; Asem et al., 2014).

120 2.2. Geological setting

121 Iran lies in the Alpine-Himalayan orogenic belt. The North-West of the country, where Lake
122 Urmia is located, is a part of the Turkish–Iranian Plateau with an average altitude of around 2000
123 m a.s.l. and is situated in the center of the Arabian-Eurasian collision zone. The crustal
124 deformation since the upper Miocene is dominated by N-S shortening and E-W extension
125 (Berberian and Arshani, 1975, Solaymani, 2009). This resulted in faulting, seismic activities and
126 the forming of volcanoes which are the highest mountains on the plateau. As other lakes in the
127 area, Lake Urmia is located in a tectonic depression related to the large zones of faulting. The
128 Tabriz fault system limits this depression to the North-East while the Sahand volcano (3695 m
129 a.s.l.; 3rd highest volcano on the plateau), dominates the east of the lake area. About 100 km to
130 the west of the lake lies the active Zagros thrust belt. This tectonic activity results in intense
131 seismicity. The archives show that since 600 BC, more than 450 big earthquakes happened in the
132 region. Recent and historic data since 858 AD record a high seismic activity in the area of Urmia,
133 especially associated with the Tabriz fault. In this time span, at least 12 major catastrophic
134 earthquakes destroyed the town of Tabriz (Solaymani 2009).

135 Lake Urmia catchment area is composed of rocks ranging from Precambrian to Quaternary.
136 Volcanic and volcano-sedimentary formations dominate in the east and northeast of the
137 catchment area. Intrusive rocks, as well as metamorphic rocks, are mainly found in the south,
138 west, and northwest (Fig. 1d). Carbonate sedimentary units are mainly found in southern and
139 western parts, and evaporite sedimentary units are present to the northeast of the watershed area.
140 According to Kelts and Shahrabi (1986), Lake Urmia sediments are principally composed of
141 detrital particles of varying grain size (clays-silts-sand-gravel), chemically precipitated aragonite,
142 shrimp fecal pellet sands, thin aragonite crusts, ooids, and evaporites.

143 3. Materials and methods

144 3.1. Material collection

145 During the fieldwork campaigns in 2016 and 2017, seven sediment cores (0.6 m to 14.2 m long)
146 have been drilled out from recently dried out part of the lake near the city of Urmia. Water
147 sampling and in-situ measurements were performed on the lake and river as well as on
148 groundwater (Fig. 2, Tab. 1). The shortest 0.6 m long core Golman 4 has been taken manually,
149 directly to the plastic tube and close to the today's lake shoreline, for the retrieval of the lake-
150 sediment interface. This provided a sampling of the undisturbed, continuous top sedimentary
151 sequence of the lake. Six other cores have been taken with a mechanic corer and casing of the
152 borehole at a distance from the today's shoreline allowing safe using of the corer. Therefore, all
153 cores have been taken from the recently dried out lake bottom (Fig. 2a). Below the surficial crust,
154 the uppermost sediment was soft sand-rich, and was collected either as compacted (Golman 5 and
155 Golman 6) or incomplete sequence (Golman 3 and Golman 7). The two longest cores, *i.e.*
156 Golman 3 and Golman 7, were empty in their middle part; too liquid, either sandy or clayish
157 sediment being impossible to be taken out, the solid lower sequence was lightly compacted
158 during coring. When coring reached the depth of ~5 m, H₂S gas began bubbling (Fig. 2b).
159 Corings Golman 3 and Golman 7 were stopped when pressurized water with mud and gas with an
160 intense H₂S odor rose up from the boreholes to the sediment surface. Cores Golman 1 and
161 Golman 2 were very incomplete and only small and disturbed fragments of sediment were
162 collected but not analyzed. In-situ parameters such as temperature, pH and conductivity have
163 been measured on surface water (Lake Urmia and Shahr Chai River at several locations) and on
164 groundwater (rising-up muddy water from coring wells as well as 6 surrounding wells distributed
165 according to a potential flow line). Samples from all water points have been taken for chemical
166 (major anions and cations) and stable isotope analyses (¹⁸O_{water}, ²H_{water}). During fieldworks, we
167 observed important lake water level changes both in seasonal and annual scale. In May 2016, the
168 lake water level decreased by ~1m just due to the end of the winter/spring intense rainfall period

169 and the increase of the evaporation rate (Fig. 2c). In September of 2017, the water level had
 170 lowered so that the lake water sampling sites from 2016 had become dry (Fig. 2d).

171 3.2. Methods

172 On the field temperature, water electric conductivity and pH of were measured with WTW 3210
 173 conductivity meter and pH-meter respectively. Sediment characteristics have been obtained
 174 through laboratory analyses as presented below.

175 3.2.1. Measurements of water contents and salinity

176 Water content in sediment was obtained through the difference of weighted humid, immediately
 177 taken from fresh core sediment samples and the same samples weighted after drying for three
 178 days at 80°C in a laboratory oven.

179 The salinity measurements had to take into account the fact that salt is present both in the solution
 180 and in the solid part of sediment. Therefore, the total salt content was obtained by washing the
 181 salts from the dried out sediments three times with distilled water and weighting the remaining
 182 dried fraction. The difference between the mass of dried out sample and the mass of the dried out
 183 sample after washing gives the quantity of salt which we normalized by the water content. In the
 184 following equation, the numerator corresponds to the quantity of soluble material washed out of
 185 the sediment and the denominator to the water content.

$$186 \quad S = \frac{W_{Bdry} - W_{WOdry}}{W_B - W_{Bdry}}$$

187 Where:

188 W_B , mass of bulk fresh sample

189 W_{WOdry} , mass of washed out and dried sample

190 W_{Bdry} , mass of bulk dried sample

191 3.2.2. Grain size, carbonate content and bulk sediment mineralogy

192 Grain-size distribution measurements of organic matter and carbonate-free sediment were carried
193 out on a Malvern Mastersizer 2000 apparatus. The carbonate content ($\text{CaCO}_3 + \text{MgCO}_3$) was
194 obtained using a Mélières mono-calcimeter: 100 mg of dried and homogenized bulk sample was
195 reacted with 3 mL of 1 N hydrochloric acid (HCl) in a closed vessel and the resulting pressure of
196 CO_2 gas was measured by a manometer. The calibration was conducted by reacting 100 mg of
197 pure calcium carbonate as standard with 3 mL of 1 N HCl, implying a 1 atm pressure read on the
198 manometer. These measurements were done at GEOPS laboratory (University Paris-Saclay,
199 Orsay, France).

200 Identification of mineralogical components was performed by XRD on the whole sediment
201 powder at GEOPS laboratory. The XRD pattern was recorded with an X'Pert Pro PANalytical
202 diffractometer, Cu-K \rightarrow source, 2θ range 5° - 80° , 4-h runs and identification phase using
203 PANalytical HighScore software and crystallography open database following the laboratory
204 routine at GEOPS laboratory. Specific carbonates were identified through analyzes during 45
205 minutes with 2θ range 24° - 33° . The semi-quantification of the carbonates was obtained by
206 normalizing the areas of the diffraction peaks with respect to the percentage of areas coming from
207 an equi-mass mixture of carbonates, then setting the ratio of the normalized area of each
208 carbonate to the sum of the standardized areas.

209 3.2.3. Magnetic parameters

210 Low field magnetic susceptibility (\blacktriangledown) was measured with a Bartington Instruments MS-2
211 susceptibility bridge directly on the sediment surface of the half-core. The thermomagnetic
212 behavior of the bulk sediment samples was determined on a horizontal force translation Curie
213 balance. Analyses were performed under normal air atmosphere, in a magnetic field of 0.375 T
214 and with a linear temperature increase of $10^\circ\text{C min}^{-1}$. The XRD pattern of the magnetic extracts
215 was recorded with an X'Pert Pro PANalytical diffractometer, Cu-K \rightarrow source, 8-h runs and
216 Panalytical Low background substrate, *i.e.* a 32-mm silicon single crystal substrate for

217 measurements of small amounts of sample material that require low background intensity.
218 Magnetic susceptibility, XRD and Curie balance experiments were carried out at GEOPS
219 laboratory. Magnetic hysteresis measurements of the bulk sediment samples were performed at
220 room temperature with an alternating gradient magnetometer (AGM 2900 – Micromag) at LSCE
221 laboratory, CNRS/CEA at Gif-sur-Yvette, France. A peak - applied field of 1 T was used for
222 hysteresis measurements. The values of saturation magnetization (M_s), saturation remanent
223 magnetization (M_{rs}) and coercive force (B_c) were estimated from the slope corrected hysteresis
224 loop. Parameters M_s and M_{rs} were mass normalized. Coercivity of remanence (B_{cr}) was
225 obtained by step-wise application of back-fields to remove the saturation remanence.
226 Magnetic susceptibility was measured on all sediment cores while other parameters were
227 measured systematically on core Golman 7 and additionally in some other sequences.

228 3.2.4. Radiochronology

229 Six AMS datings have been done on organic fractions (diffused organic matter and hand-picked
230 charcoal).
231 Each fraction has been submitted to the standard chemical protocol for AMS analyses for organic
232 remains, *i.e.* cleaning treatment via successive hydrochloric acid/sodium hydroxide/hydrochloric
233 acid baths respectively, and rinsed with deionized water up to neutral pH. Samples were then
234 gently dried at 60°C overnight. CO₂ gas was obtained according to the AMS protocol of burning
235 at 860 °C for 30 min, under vacuum, in presence of a mixing of copper(II)-oxide/copper(III)-
236 oxide and silver thread. Then, AMS-¹⁴C targets were obtained by graphitization of the CO₂ gas on
237 powdered iron with hydrogen at 650 °C for 100 min, and graphite compression under analytical
238 plots. Aliquot of the CO₂ gas was then used for associated ¹³C measurement. These were
239 measured on a VG SIRA 10 IRMS (Isotope Ratio Mass Spectrometer) at the GEOPS laboratory.
240 Graphite sources were also prepared at GEOPS laboratory, and counted by the accelerator mass
241 spectrometer at LSCE laboratory (ECHO MICADAS facility, France).

242 Analytical uncertainties, including laboratory errors, are $\pm 0.1\%$ for $\delta^{13}\text{C}$ and between 0.5 and 0.8
243 pMC for ^{14}C activity. All the dates are converted to calendar ages according to the revised
244 calibration program CALIB 7.10 (Reimer et al. 2013, Execute Version 1.10html 2020).

245 4. Results

246 4.1. Water measurements

247 Results of in-situ measured electric conductivity (EC), pH and temperature on surface water and
248 groundwater are presented in the Table. 1. At a first glance, data from both field campaigns (May
249 2016 and September 2017) show that lake's basin waters present a wide range of EC values,
250 varying from 0.25 mS.cm^{-1} for the Shahr Chai River far from the lake, to 227 mS.cm^{-1} for the
251 coring muds. Considering the flow line of the Shahr Chai River, the conductivity and temperature
252 remain low close to its source above the dam and in the city of Urmia (0.30 and 0.25 mS.cm^{-1} ,
253 $\sim 14^\circ\text{C}$, respectively) and increase between the city and the river outlet (3.40 mS.cm^{-1} and $\sim 17^\circ\text{C}$
254 respectively) while pH shows opposite trend. Groundwater from wells presents temperatures
255 varying between 14.2 and 19.9°C , pH evolving from 6.1 to 8.1 and conductivity comprised
256 between 0.58 and 12.39 mS.cm^{-1} . Lake surface water temperature reaches even 28°C ; its
257 conductivity and pH are respectively $\sim 200 \text{ mS.cm}^{-1}$ and 7.5 to 8.0 , depending of the measurement
258 site. Groundwater (more or less muddy) rising up to the sediment surface in the boreholes,
259 presents very high conductivity and relatively low pH.

260 Water samples taken upstream from the town of Urmia show EC values in agreement with
261 drinking water standards, either of good quality (until 0.80 mS.cm^{-1}) or acceptable (up to 2.50
262 mS.cm^{-1} at a maximum; Drinking Water Directive of European Commission, 2021). About 10 km
263 downstream from Urmia city and towards the lake, EC values evolve from 3.40 mS.cm^{-1} to 207.0
264 mS.cm^{-1} , indicating an increase in the evaporation rate. Three of the wells used for drinking water
265 until 2016 are now abandoned. Lake Urmia brine's points out a measured conductivity of 207
266 mS.cm^{-1} . Such a high conductivity has been also found in waters rising up from coring wells, and

267 likely representing captive brines they are markers of ancient lake state. In a pH vs EC diagram
268 (Fig. 3a), two different clusters of conductivity are highlighted and in relation with the two
269 captive brines values. The first (A) displays mean value of $221 \pm 4 \text{ mS.cm}^{-1}$ and characterizes
270 waters rising steeply from intermediated depths during coring (below 4.5-5 m), while the second
271 one (B), with mean value of $146 \pm 8 \text{ mS.cm}^{-1}$, characterizes highly pressurized water coming
272 from the bottom of core Golman 3. Similar pressurized water was coming from the bottom of the
273 Golman 7 coring tube but unfortunately could not be sampled.

274 4.2. *Sedimentary record*

275 Sediments obtained from cores Golman consist of fine – silty/clayish and sandy deposits with
276 some gravel levels and some sections that contain ooids and fecal pellets of the brine shrimp
277 *Artemia urmiana* (Fig. 2e-h). The shortest core Golman 4 (Fig. 2e, Fig. 4a) presents continuous
278 sequence of top 0.60 m sediment. The cores Golman 3 and Golman 7 are, respectively, 14.20 and
279 12.50 m long sequences but present an important gap in the middle due to the liquidity of sandy
280 and clayish/silty sediments (Fig. 4c and d). Sedimentary sequences of both cores display the same
281 pattern although Golman 7 is more complete. Sequences of the cores Golman 5 and Golman 6 (3
282 and 8 m long, respectively, Fig. 4b, e), are in good agreement with those for cores Golman 4 and
283 Golman 7. Moreover, the section between 8.00 and 4.20 m depth of the core Golman 6 completes
284 the gap in the core Golman 7 (Fig. 4f,g), both cores have been collected very close to each other
285 (Fig. 2a).

286 4.2.1. Correlations between cores, reconstruction of the composite core and lithology

287 The reconstruction of a complete sequence is based on detailed sedimentary description,
288 carbonate contents and magnetic susceptibility, and the correlation, in a reliable and precise way,
289 of characteristic levels between different cores. This composite sequence will allow us to
290 integrate, and therefore to interpret, all the data on a single stratigraphic sequence.

291 In the uppermost part of the lake sedimentary sequence (i.e. core Golman 4; Fig. 4a), the
292 magnetic susceptibility relatively high in the lower, sandy part of the section, decreases at ~0.20
293 m depth and stays low to the top in fine grained sediments while the carbonate contents present
294 the inverse evolution, i.e. low at the beginning and increasing up to ~0.20 m depth. Similar
295 pattern and change are recorded in the core Golman 5 at ~1m depth (Fig. 4b). Above this change,
296 in both cores, fecal pellets are very abundant. Magnetic susceptibility of the upper sediment in
297 cores Golman 3, 5, 6 and 7, shows varying values with an increase at the depth of ~3 m that is
298 easily correlated between all cores and is highlighted by a grey band on Fig. 4. This increase
299 corresponds to the presence of blackish sandy sediment rich in organic remains, and to the
300 decrease of the carbonate contents recorded in cores Golman 5 and Golman 7 (Fig. 4b, d). Three
301 different changes of the magnetic susceptibility below this section are indicated by grey lines on
302 Fig. 4. The increased magnetic susceptibility recorded in the lowermost sediments of cores
303 Golman 3 and Golman 7 as well as pressurized water and gas rising from the bottom to the
304 sediment surface there, allow the correlation of both beginnings of cores. The highest value of the
305 susceptibility was recorded at ~1 m depth in the sandy sediment of the core Golman 3. This, due
306 to a piece of a broken corkscrew found in this level during sediment sampling, clearly indicates
307 modern age for this sediment (Fig. 4c).

308 Cores Golman 7 and Golman 6 display the complete sequence of the sediment from 12.5 to 1.60
309 m depth. The sediment between 12.50 and 12.38 m depth is sandy (Fig. 2f) and silty. The color of
310 the lowest, sandy ~2 cm layer is light brown while above, it is black and rich in plant remains
311 (between 12.47-12.44 m) and dark grey. From 12.38 to 4.52 m depth, the sediment consists of
312 quite soft and grey silt/clay (Fig. 2g), with some fine (~1 mm thick), dark grey sandy laminae.
313 After a clear change at 4.52 m, the upper sediment is more complex with alternation of sands,
314 silts and clays of different colors and some discontinuities. The 4.52 - 3.73 m interval presents
315 brownish, coarse silty quite compact sediments (4.52 - 4.02 m), clayish/silty grey and brown
316 deposits (4.02 - 3.85 m) and dark grey sand (3.85 - 3.73 m). Above, between 3.73 and 2.87 m

317 depth, the sediment is quite homogeneous, made of grey fine silt and clay that is very rich in
318 shrimp's fecal pellets (Fig. 2h). It begins as a hard 2 cm thick horizon clearly separated from
319 lower dark grey sand, and becomes quite soft in the middle. The last few centimeters are light
320 grey, quite dry and end sharply at 2.87 cm depth below the 8 cm thick black and sandy sediment
321 that is rich in organic remains including plant fragments. Above, the sandy sediment, more or less
322 dark and devoid of fecal pellets, continue until 2.20 m. The upper 2.20-1.60 m sands and silts
323 contain varying concentrations of fecal pellets.

324 4.2.2. Radiochronology

325 Four ^{14}C AMS datings have been obtained from charcoal and two others, from organic matter
326 (Table. 2). Dating for core Golman 7 present ages of 29.70, 18.34 and 5.52 cal kyr BP at 12.46
327 m, 4.05 m and 2.80 m depth respectively. Two additional dating performed on core Golman 5 at
328 2.66 and 2.34 m depth, display ages of 4.95 and 4.90 cal kyr BP respectively. These two dated
329 samples represent the same blackish unit with high magnetic susceptibility values as the one in
330 recognized in core Golman 7 at 2.80 m depth (Fig. 4). Finally, the core Golman 6 sample at 4.40
331 m depth indicates 21.20 cal kyr BP. This sample and the 4.05 m depth sample from the core
332 Golman 7 belong to the same lithological unit (Fig. 4).

333 Although we were not able yet to determine whether the lake water is submitted to a hard water
334 effect or not, the strong winds existing the region allow the good mixing of the lake water: in
335 such a system, we may consider at a first glance that the lake water total dissolved inorganic
336 carbon (TDIC) is in equilibrium with the atmospheric CO_2 (MacDonald et al., 1991; Fontes et al.,
337 1993, 1996; Gibert et al., 1999, 2002a, 2002b; Schneider et al., 2019). However, in order to avoid
338 as much as possible any suspicion of bias in our datings, we thus concentrate on authigenic
339 materials (i) without any link with the carbon lake system such as charcoal, and (ii) with a high
340 C-content for planktonic organic matter and no indication of a detrital origin (mineralogical
341 assemblages). All the ^{14}C datings presented are thus considered as fully reliable.

342 All these datings are in agreement with the stratigraphy (Fig. 4, Fig. 5). Without any information
343 on the hydrogeochemical balance of the sub-basin of the cored sequences, the interpretation of
344 the ^{14}C datings is only discussed within the framework of the internal consistency of the whole
345 chronology with respect to the lithological sequences.

346 Moreover, the dated samples present associated ^{13}C contents ranging from -26.50 to -13.50 ‰ vs
347 PDB with a majority of the samples being centered on a value of -25.2 ‰ vs PDB. This value
348 highlights the predominance of a C3 vegetation over Lake Urmia catchment. The G5-2.34 sample
349 presents a $\delta^{13}\text{C}$ value corresponding to a C4 vegetation while sample G7-S2-2.80 exhibits two
350 distinct $\delta^{13}\text{C}$ values of -13.5 and -26.5 ‰ vs PDB. This latter is explained by the mixing of two
351 fractions of micro-charcoal, one originating from C3 plants and one from C4 plants, both
352 coexisting in the lake basin (including the lake itself, Decolas-Gros, 1985.) at the time of
353 deposition.

354 4.2.3. Sediment characteristics

355 Water contents, salinity and grain size:

356 Water contents in the sediment display values between 12 and 37% (Fig. 5c), and, as commonly
357 seen, are likely correlated to the grain size; lower water percentages characterising sandy
358 sediments while higher ones correspond to the silty/clayish levels. The calculated salinity
359 indicates relative changes of the total dissolved salts present in interstitial water and sediment.
360 The obtained pattern indicates less salinity in the lower part of the core, as well as at ~3.90 m and
361 between 3.65 and 2.20 m depth, and higher but changing salinity elsewhere (Fig. 5d). Mean grain
362 size values vary between ~10 and ~160 μm , with a dominant fine silty fraction in the lower part
363 of the core and silty and sandy sediments in its upper part (Fig. 5e). High water contents and low
364 sediment grain sizes, characterize the sequence between 12.38 and 4.52 m depth, from 4.02 to
365 3.85 m and between 3.73 and 2.87 m depth. These fine-grained sediments are well correlated
366 with the relatively low water salinity. Sandy/silty sediments that are less humid are present at the

367 bottom of the sequence at ~12.50 m depth and in some horizons of its upper 4.52 m (4.52-4.02 m,
368 3.85-3.73 m, 2.87-2.40 m, and 2.20-1.60 m depth).

369 Mineralogy and carbonate contents: XRD mineralogy on bulk sediment has been done on 41
370 samples from cores Golman 3 and Golman 7. Minerals that are identified in all levels are quartz,
371 muscovite, halite and calcite, the two former representing the siliceous detrital fraction. Other
372 carbonates such as aragonite and dolomite were identified in most of the samples. Carbonate
373 contents vary between ~7 and ~66% of the total sediment (Fig. 5f). When existing, aragonite
374 dominates the carbonate fraction and reaches even 65% while calcite and dolomite have low to
375 very low contents varying between 1 to 12% for calcite and around 2% for dolomite (Fig. 5g).
376 Aragonite can be related to the chemical or biochemical precipitation such as calcite, although
377 calcite can be of detrital origin too. Dolomite originates from either chemical precipitation or
378 detrital supply. Microscopic observations and analyses on Lake Urmia sediment by Kelts and
379 Shahrabi (1986) show the predominance of aragonite in the lake sediments. These authors
380 indicate that aragonite is present as mud and at least composes ~80% of the carbonate as shrimps
381 fecal pellets. In our core, aragonite varies greatly and reaches even 65% between 3.73 and 2.87 m
382 depth where shrimp's fecal pellets are particularly abundant.

383 Magnetic parameters: magnetic susceptibility presents clear changes with alternating sections of
384 low and high values (Fig. 5a). The magnetic hysteresis parameters as M_r/M_s versus H_{cr}/H_c for
385 samples from cores Golman 7 and Golman 5 are presented in the Day diagram (Day et al., 1977,
386 Fig. 3b). It shows the distribution of the magnetic particle grain sizes in three clusters: SD -
387 magnetic single domain sizes with typical hysteresis loop shape as on Fig. 3d, MD - multi-
388 domain, with hysteresis loop as on Fig. 3c, and PSD - pseudo-single-domain intermediated sizes.
389 The PSD and MD sizes are present in the low magnetic susceptibility sediments; generally, the
390 MD are present in sandy, while PSD, in fine silty ones. The thermomagnetic behavior of samples
391 with PSD and MD magnetic minerals during heating shows clearly the Curie temperature at
392 580°C indicating the presence of magnetite (Fe_3O_4), an iron oxide, in the sediments (Fig. 3e). For

393 samples with SD magnetic particles that are mostly correlated with high values of magnetic
394 susceptibility, the Curie balance experiments during heating show a magnetization decrease at
395 $\sim 350^{\circ}\text{C}$. This process is irreversible due to the appearance of new magnetic mineral that is
396 observed during cooling (Fig.3f). Such a behavior is characteristic for greigite (Fe_3S_4), an iron
397 sulfide (Jelinowska et al., 1997, 1998, 1999; Strechie et al., 2002; Tudryn et Tucholka, 2004;
398 Tudryn et al., 2013, 2014), whose presence is confirmed through XRD analyses of total sediment
399 and magnetic extracts for the concerned depths (Fig. 3g). Magnetic susceptibility presents a
400 correlated pattern to the mean grain size and anti-correlated ones to the carbonates and water
401 contents with however, some independent peaks at sandy/silty depths of ~ 12.45 m and at ~ 2.80
402 m, and larger, silty/clayish section between 8 and 5.5 m depth (Fig. 5). The considered
403 sandy/silty sediment is black and rich in vegetation remains with numerous pieces of wood while
404 silty/clayish section is grey. In sediments characterized by low magnetic susceptibility values, the
405 magnetic hysteresis parameters and Curie balance experiments allowed the identification of low
406 contents of MD and PSD magnetite (squares and circles on Fig. 3b and circles on Fig.5b) that is
407 of detrital origin while in sections with high magnetic susceptibility, SD greigite appears (black
408 triangles on Fig. 3b and Fig. 5b). Greigite is an iron sulfide of early diagenetic origin: it is an
409 intermediated mineral in the authigenesis of the pyrite during the bacterial degradation of the
410 organic matter in the anoxic, sulfate-reducing zone of the sediment or water, where the S/Fe ratio
411 is too low to complete the pyritisation process (Berner, 1980; Curtis, 1987). The presence of
412 greigite is surprising in such a saline environment as Lake Urmia, where sulfate ions are
413 abundant in water. Nevertheless, greigite is well known from other hypersaline lakes as Manas in
414 China (Jelinowska et al., 1995, Tudryn et al. 2010), Dead Sea (Frank et al., 2007) and salt
415 marshes (Cutter and Velinsky, 1987). The presence of greigite in such environments is related to
416 the fresh water supply, high organic matter content or, if methane is present in the environment,
417 an anaerobic oxidation of methane by sulfate reduction (either bacterial or not bacterial; *e.g.*
418 Avrahamov et al., 2014, Neretin et al., 2004). As in Lake Urmia, early diagenetic greigite was

419 often associated with black sediment that is rich in plant fragments including pieces of wood (at
420 depths of ~12.45 m and ~2.80 m), it is related to the bacterial degradation of the organic matter in
421 the anoxic, sulfate-reducing zone rather than to methane oxidation.

422 **5. Discussion**

423 As indicated by all our proxies and during all the time covering the sedimentary sequence, the
424 detrital minerals such as quartz and muscovite have been supplied to the lake and evaporitic
425 conditions, with saline waters and precipitation of halite, were prevailing in the Lake Urmia. The
426 electric conductivity of two-captured brines at different depths during coring highlights changes
427 of its salinity in the past.

428 The sequence starts with sandy deposits indicating either a high-energy transport related to the
429 fluvial activity of River Shahr Chai or a low water level at the place of coring. The light brown
430 color of the sand and the presence of detrital magnetite (that is MD and in low contents) highlight
431 well oxygenated conditions during the sedimentation. In these deposits, pressurized gas and brine
432 are captured. The brine shows lower electric conductivity than today's lake waters and thus, less
433 water salinity. A few centimeters above the bottom of the core, at ~30 cal kyr BP (12.46 cm
434 depth), the deposits become black, silty, with some calcite and dolomite but without aragonite.
435 They are rich in authigenic greigite and plant remains that, according to $\delta^{13}\text{C}$ (Table 2), are
436 identified as C3 plants. The former iron sulfide indicates the anoxic and sulfate reducing
437 conditions within the sediment. The high content of organic material here could reflect an
438 increased input of organic detritus through the river, nevertheless the decreased grain size of the
439 sediment and its bad oxygenation suggest the development of a salt marsh with high biological
440 productivity rather than a high river activity. Such a start of the sedimentary sequence reflects
441 quite low lake water level, without lacustrine or very shallow condition in the coring area (Fig.
442 5). The above ~8 m thick sequence between 12.38 to 4.52 m depth is quite homogeneous, grey
443 and with high water content. The fine-grained sediment indicates that it was deposited in low
444 energy transport conditions. In this section, carbonate contents reach values of ~20 to 30%. Some

445 2-3 % of carbonates, either calcite or dolomite, can be of detrital origin according to the
446 distribution of carbonate rocks in the River Shahr Chai catchment area (Fig. 1d). Nevertheless,
447 most of the carbonates are authigenic or bio-mediated as evidenced by the dominance of
448 aragonite mud in the carbonate fraction. According to Kelts and Shahrabi (1986), precipitation of
449 aragonite rather than calcite is a function of the high Mg/Ca molar ratio. Relatively low pore-
450 water salinity values suggest less saline conditions than in the upper part of the sediment. All
451 parameters provide a coherent indication of higher water level than in the beginning of the
452 sequence, and high enough to show clearly lacustrine conditions at the coring site. The magnetic
453 fraction of this sediment is dominated by detrital, PSD magnetite in its lower part until ~8 m
454 depth, and by greigite above. Greigite indicates early diagenetic, sulfate reducing processes in
455 anoxic sediment and possibly bad ventilation of the bottom water, in good agreement with high
456 lake level. The presence of magnetite could be interpreted as indicating the good ventilation of
457 the basin during its deposition (between 12.38 and 8.00 m), as at the beginning of the sequence at
458 12.50 m depth where light brown sand with MD magnetite is present and the PSD magnetite here
459 could reflect the different source of the detrital material. Nevertheless, quite homogeneous
460 conditions recorded between 12.38 m and 4.52 m, grey color of the sediment and greigite present
461 above 8.00 m (Fig. 2g, Fig. 5) suggest rather anoxic early diagenetic conditions in the magnetite
462 bearing sediments. These conditions without sulfate reduction allowing the iron sulfides
463 precipitation, could favor bacterial reduction of iron oxydes (Curtis, 1987) that resulted in the
464 decrease of their grain size from MD to PSD without their complete dissolution.

465 These data indicate thus Lake's Urmia low stand at ~30 cal kyr BP. Afterwards the lake level
466 increased and stayed high, probably the highest recorded since that time until today. According to
467 the ¹⁴C dating, it finished before 21.20 cal kyr BP (Fig. 5). Djamali et al. (2008a) proposed a high
468 lake water level during the last glacial period while Stevens et al. (2012) indicated a clearly arid
469 climate at Urmia at that time associated to a low lake level and no establishment of a perennial
470 saline lake until ~ 14 kyr. A high stand during the considered part of the glacial period is reported

471 in the region from other lakes such as Lake Zeribar (Wasylikowa et al., 2006) and Lake Van
472 (Kuzucuoglu et al., 2010).

473 The pattern of all parameters displays several changes in the upper part of the sequence and
474 discontinuities are observed (Fig. 5). It starts, between 4.52 and 4.05 m depth, with water content
475 decreased, brown sandy/silty low-carbonated sediments that contain MD magnetite, and
476 relatively high salinity probably highlighting a low lake level and well oxygenated environment.
477 According to ^{14}C dating, this low lake stand is recorded between 21.2 and 18.3 cal kyr BP and
478 corresponds to the Last Glacial Maximum (LGM). After that, short-time lacustrine conditions
479 indicated by fine sediment grain sizes, decreased water salinity and increased carbonate contents
480 including aragonite mud (up to 20%) were identified between 4.02 - 3.85 m depth before a
481 lowering between the depths of 3.85 – 3.73 m marked by increased sediment grain sizes and
482 water salinity, and decreased carbonate contents without aragonite. The presence of MD
483 magnetite indicates well oxygenated environment. The re-establishment of clear lacustrine
484 conditions between 3.73 and 2.87 m depth were recorded by fine-grained sediments, carbonate-
485 rich fraction with very high contents of aragonite and abundance of shrimp fecal pellets (Fig. 2h).
486 The presence of some greigite and PSD magnetite, suggest bad ventilation of the bottom water.
487 The beginning and end of this section are marked by sharp change in the lithology, grain size,
488 magnetic susceptibility, carbonate contents and mineralogy. Its lower limit highlighted by the ~2
489 cm thick dried grey sediment, as well as its upper part clearly indicate drying up, and both limits
490 suggest discontinuities in the sedimentation. Above 2.87 m and until ~2.2 m depth, dark sandy
491 and silty sediment with low carbonate contents but without aragonite was deposited. Between
492 2.87 and 2.77 m depth, it is black and particularly rich in organic remains and greigite. According
493 to the radiocarbon data of this black sediment, this episode started at ~5.5 cal kyr BP and lasted
494 until at least ~4.9 cal kyr BP. This sediment suggests similar lake low stand to that recorded at
495 the beginning of the sequence *i.e.* at ~30 cal kyr BP, without lacustrine or very shallow condition
496 in the coring site. Moreover, the dated samples exhibit two distinct $\delta^{13}\text{C}$ values of -26.5, -25.50

497 ‰ and of -13.5, -14.50 ‰ vs PDB (Table 2), the first originating from C3 plants and the second
498 from C4 plants, both coexisting on the watershed at the time of deposition. We observed that the
499 C4 vegetation episode that seems to have lasted at least 600 years, between 5.5 and 4.9 cal kyr
500 BP likely indicates a warmer and drier episode. The latest recorded sandy sediment rich in shrimp
501 fecal pellets (2.20-1.60 m), reflects a lacustrine episode with River's Shahr Chai high energy
502 transport at the place of the coring site. Today, the downstream electric conductivity
503 measurements of River Shahr Chai and of lake water indicate an increase in the evaporation rate
504 with its very high values for the lake. These results are in good agreement with our first
505 hydrogeochemical results on the water samples (E. Gibert-Brunet, pers. comm., Kong et al.,
506 2019). According to these results, including rivers and surrounding wells, the lake is fed not only
507 by direct precipitations and inflow of rivers, but also by groundwater discharge. This present-day
508 discharge has very likely evolved over time in relation with the lake level and could have been
509 more important during the first phases of lake level drop.

510 According to ¹⁴C dates, Lake Urmia evolution from the LGM until today was characterized by
511 lake level fluctuations with three high and three low stands recorded at the coring site (Fig. 5).
512 Kelts and Shahrabi (1986) identified, in the ~4 m thick sedimentary sequence from South Lake
513 Urmia basin, three lacustrine high stands that they named "Aragonite-Pellet-Mud" (APM) and
514 two low ones stamped "Playa-Lake-Mud" (PL). Authors highlighted the lack of readily dateable
515 material in their study, but proposed ~9-7.5 kyr BP for the lake high stand APM-2. This Early
516 Holocene timing is in good agreement with the relatively long-term lacustrine conditions we
517 recorded before ~5.5 cal kyr BP. Previous study by Stevens and coauthors (2012) in the eastern
518 part of Lake Urmia described dry condition during the Late Pleistocene with a short-term
519 lacustrine episode at ~14 kyr, drying out probably in phase with the Younger Dryas and no re-
520 establishment of lacustrine conditions until ~ 10 kyr. Holocene reconstructions by Sharifi (2018)
521 suggested wet Early Holocene and frequent dry episodes during Mid to Late Holocene.

522 Contrary to the lacustrine records from Zagros Mountains (lakes Zeribar, Mirabad, Dasht-e
523 Arjan) that indicate dry conditions and low lake levels during the Early Holocene (Stevens et al.,
524 2006; Wasylikowa et al., 2006; Aubert et al., 2019), clearly lacustrine conditions dominated in
525 Lake Urmia at that time. Such wetter conditions than those prevailing in the Zagros area, as well
526 as changing ones during the Late Holocene, are in good agreement with data from Lake's Neor
527 area, located in the NW Iran (Sharifi et al., 2015; Aubert et al., 2017).

528 Transition from Early to Late Holocene in Lake Urmia, was marked by a low lake level and thus
529 dry conditions between ~5.5 and ~ 4.9 cal kyr BP. Such a dry event was identified during broadly
530 the same time in Zagros Mountains (Stevens et al., 2006) and in Anatolia (Fontugne et al., 1999).
531 It is probably linked to the drought event recorded at 5.2 kyr BP that was evidenced in the Soreq
532 speleothem record (Bar-Matthews et al. 1997) and in many others sites (see in Staubwasser et
533 Weiss, 2006). Jones and co-authors (2013) pointed out the scarcity of information and the
534 problems with identification and timespan of this event in Iran; the complex interplay between
535 natural conditions and humans during much of the Holocene in Iran makes this information
536 difficult to obtain.

537 **6. Conclusion**

538 The sediment cores collected from the SW part of Lake Urmia close to the city of Urmia
539 represent a Late Pleistocene and Holocene record of the paleohydrological evolution of the lake.
540 Our proxies indicate that during the whole deposition period of the sedimentary sequence, the
541 detrital minerals, such as quartz and muscovite, have been supplied to the lake. Aragonite (if
542 present in the sediment) dominated the carbonate fraction and evaporitic conditions with saline
543 waters and precipitation of halite, were prevailing in the lake.
544 Our established timescale is based on 6 reliable ¹⁴C datings that give chronological anchors for
545 the presented data. A low stand of the lake was identified at about ~30 cal kyr BP (and even
546 drying out at the coring site) and followed by a water level rise leading to establishment of
547 lacustrine conditions, with probably the highest water level from that time until today. According

548 to the ^{14}C dating, the water level decreased prior to the LGM. Lake evolution from the LGM until
549 today was characterized by several changes of the water level with clearly lacustrine conditions
550 and lake low stands. Between ~ 5.5 and 4.9 cal kyr BP, the lake experienced low stand and even
551 drying out at the coring site. Just before this, during the Early Holocene, relatively long-term
552 lacustrine conditions were established.

553 Sediments from two dry events at the coring site recorded at ~ 30 and at 5.5 - 4.9 cal kyr BP are
554 characterized by high contents of authigenic greigite associated to the organic matter rich
555 environment. Elsewhere, in sandy sediments, low contents of MD detrital magnetite are present
556 while in fine grained ones, PSD magnetite or greigite dominate. These changes of the magnetic
557 mineralogy reflect differences in the oxygenation state of lake sediment and water.

558 Our work has allowed presenting a Late Pleistocene and Holocene record of the
559 paleohydrological evolution of Lake Urmia based on the valuable material collected, including
560 sediments and water. Those first results open a wide possibility for further analysis and
561 crosschecking, associated to the strengthening of the ^{14}C chronology to establish a high temporal
562 resolution of the lake evolution. The pluridisciplinary study of Lake Urmia basin will enable to
563 extend the discussion on environmental changes to the regional scale.

564 **7. Acknowledgement**

565 This work was supported by the French-Iranian project Gundishapur, the Center for International
566 Scientific Studies and Collaboration (CISSC), TelluS Program of CNRS/INSU and China
567 Scholarship Council (CSC) for one of the coauthors PhD fellowship. We thank Kuadio A.,
568 Yilmaz N., Chanon C., Coulibaly S., Belarb S., Convard de Prolles A., Lezeau G. and
569 Randrianarivélo C., students from Paris Sud University who contributed to this work during their
570 Licence and Master traineeship.

571 **8. References**

- 572 Ahmady-Birgani, H., Ravan, P., Schlosser, J. S., Cuevas-Robles, A., AzadiAghdam, M., &
573 Sorooshian, A., 2020. On the chemical nature of wet deposition over a major desiccated lake:
574 Case study for Lake Urmia basin. *Atmospheric Research*, 234, 104762.
- 575 Ahmady-Birgani H., Agahi E., Ahmadi S.J., Efranian M., 2018. Sediment source fingerprinting
576 of the Lake Urmia sand dunes, *Scientific Reports*, DOI:10.1038/s41598-017-18027-0.
- 577 Alipour S., 2006, Hydrogeochemistry of seasonal variation of Urmia Salt Lake, Iran, *Saline*
578 *Systems* 2006. 2:9, doi:10.1186/1746-1448-2-9.
- 579 Asem A., Eimanifar A., Djamali M., De los Rios P., Wink M., 2014. Biodiversity of the
580 Hypersaline Urmia Lake National Park (NW Iran). *Diversity* 6:102-132.
- 581 Aubert C., Brisset B., Djamali M., Sharifi A., Ponel Ph., Gambin B., Akbari Azirani T., Guibal
582 F., Lahijani H., Naderi-Beni A., de Beaulieu J.-L., Pourmand A., Andrieu-Ponel V., Thiéry A.,
583 Gandouin E., 2017. Late Glacial and Early Holocene hydroclimate variability in northwest Iran
584 (Talesh Mountains) inferred from chironomid and pollen analysis. *Journal of Paleolimnology*,
585 Springer Verlag, 2017, 58 (2), pp.151-167.
- 586 Aubert C., Djamali M., Jones M., Lahijani H., Marriner N., Naderi-Beni A., Sharifi A., Ponel Ph.,
587 Gandouin G., 2019. A major hydrobiological change in Dasht-e Arjan Wetland (southwestern
588 Iran) during the Late Glacial – Early Holocene transition revealed by subfossil chironomids.
589 *Canadian journal of earth sciences*, National Research Council Canada, 56 (8), pp.848-856.
- 590 Avrahamov N., Antler G., Yechieli Y., Gavrieli I., Loye B., Saxton M., Turchyn A.V., Sivan O.,
591 2014. Anaerobic oxidation of methane by sulfate in hypersaline groundwater of the Dead Sea
592 aquifer, *Geobiology*, 12, 511-528.
- 593 Azarbaidjan Regional Mining Cooperation, 1995. Report on the Hydrochemistry of Urmia Lake.
- 594 Bar-Matthews M., Ayalon A., Kaufman A., 1997. Late quaternary paleoclimate in the eastern
595 Mediterranean region from stable isotope analysis of speleothems at Soreq Cave, Israel.
596 *Quaternary Research* 47, 155–168.

- 597 Berner R.A., 1980. Early diagenesis: a Theoretical Approach, Princeton University Press,
598 Princeton, 1980.
- 599 Bottema S., 1986. A late Quaternary pollen diagram from lake Urmia (Northwestern Iran), Rev.
600 Palaeobot. and Palynol., 47:241-261.
- 601 Curtis C., 1987. Mineralogical consequences of organic matter degradation in sediments:
602 inorganic/organic diagenesis. In: Legget JK, Zuffa GG (eds) Marine clastic sedimentology.
603 Graham and Trotman, London, pp 108–123.
- 604 Cutter G.A. and Velinsky D.J., 1987. Temporal variation of sedimentary sulfur in a Delaware salt
605 marsh, Marine Chemistry, 23, 311-327.
- 606 Day R., Fuller M., Schmidt V.A., 1977. Hysteresis properties of titanomagnetites: grain-size and
607 compositional dependence. Phys Earth Planet Inter 13:260–267.
- 608 Decolas-Gros C., 1985. La fixation du carbone inorganique par le phytoplancton marin : données
609 bibliographiques sur les carboxylases et le rapport isotopique $^{13}\text{C}/^{12}\text{C}$. VIE MILIEU, 1985, 35
610 (1): 33-41.
- 611 Djamali M., de Beaulieu J.-L., Shah-Hosseini M., Andrieu-Ponel V., Ponel PH., Amini A.,
612 Akhani H., Leroy S.A.G., Stevens L., Lahijani H., Brewer S., 2008a. A late Pleistocene long
613 pollen record from Lake Urmia, NW Iran, Quaternary Research, 69, 413–420.
- 614 Djamali, M. Kürschner, H. Akhani, H. de Beaulieu, J.L. Amini, A. Andrieu-Ponel, V. Ponel, P.,
615 Stevens, L., 2008b. Palaeoecological significance of the spores of the liverwort Riella
616 (Riellaceae) in a late Pleistocene long pollen record from the hypersaline Lake Urmia, NWIran.
617 Review of Palaeobotany and Palynology, 152, 66-73.
- 618 Djamali M., Ponel Ph., Delille T., Thiéry A., Asem A., Andrieu-Ponel V., de Beaulieu J.,
619 Lahijani H., Shah-Hosseini M., Amini A., Stevens L., 2010. A 200,000-year record of Artemia
620 remains (Crustacea, Anostraca) in Lake Urmia, NW Iran. Int. J. Aquat. Sci.,1, 14–18.

- 621 Fontes J.Ch., Mélières F., Gibert E., Liu Qing & Gasse F., 1993. Stable isotope and radiocarbon
622 balances of two tibetan lakes (Sumxi Co and Longmu Co) from 13,000 yr B.P., Quaternary
623 Science Reviews, 12, 875-887.
- 624 Fontes J.Ch., Gasse F. & Gibert E., 1996. Holocene environmental changes in Bangong basin
625 (western Tibet). Part 1 : modern setting, mineralogy, stable isotope of carbonates and radiometric
626 chronology, *Palaeoclim., Palaeogeog., Palaeoecol.*, 120: 25-47.
- 627 Fontugne M., Kuzucuoglu C., Karabiyikoglu M., Hatté C., Pastre J.-F., 1999. From Pleniglacial
628 to Holocene: a ^{14}C chronostratigraphy of environmental changes in the Konya Plain, Turkey,
629 *Quaternary Science Reviews* 18, 573–59.
- 630 Frank U., Nowaczyk N.R., Negendank J.F.W., 2007. Rock magnetism of greigite bearing
631 sediments from the Dead Sea, Israel, *Geophys. J. Int.*, 168, 921-934.
- 632 Gibert E., Travi Y., Massault M., Chernet T., Barbecot F., Laggoun-Defarge F., 1999.
633 Comparison between carbonate and organic AMS ^{14}C ages in Lake Abiyata sediments (Ethiopia):
634 hydrochemistry and palaeoenvironmental implications, *Radiocarbon*, 41(3): 251-266.
- 635 Gibert E., Bergonzini L., Massault M., Williamson D., 2002a. AMS- ^{14}C chronology of
636 continuous deposits from a crater lake (Lake Massoko, Tanzania): modern water balance and
637 environmental implications, *Palaeoclim., Palaeogeog., Palaeoecol.*, 187:307-322.
- 638 Gibert E., Travi Y., Massault M., Tiercelin J.-J., Chernet T., 2002b. AMS- ^{14}C chronology of a
639 lacustrine sequence from Lake Langano (Ethiopia): correction and validation steps in relation
640 with volcanism influence, and lake water and carbon balances, *Radiocarbon*, 44:75-92.
- 641 Jalili S., Hamidi S.A., Ghanba R.N., 2016. Climate variability and anthropogenic effects on Lake
642 Urmia water level fluctuations, northwestern Iran, *Hydrological Sciences Journal* DOI:
643 10.1080/02626667.2015.1036757.
- 644 Jelinowska A., Tucholka P., Gasse F. and Fontes J.Ch., 1995. Mineral magnetic record of
645 environment in Late Pleistocene and Holocene sediments, Lake Manas, Xinjiang, China,
646 *Geophys. Res. Lett.*, 8, 953-956.

- 647 Jelinowska A., Tucholka P. and Więckowski K., 1997, Magnetic properties of sediments in a
648 Polish lake: Evidence of a relation between rock-magnetic properties and environmental changes
649 in Late Pleistocene and Holocene sediments, *Geophys. J. Int.*, 129, 727-736.
- 650 Jelinowska A., P. Tucholka, F. Guichard, I. Lefèvre, D. Badaut-Trauth, F. Chalié, F. Gasse, N.
651 Tribovillard and A. Desprairies, 1998. Mineral magnetic study of Late Quaternary South Caspian
652 Sea sediments: palaeoenvironmental implications, *Geophys.J.Int.*, 133, 499-509.
- 653 Jelinowska A., Tucholka P. and Badau-Trauth D., 1999. Magnetic mineral variations of South
654 Caspian Sea sediments at laminae scale. *Phys. Chem. Earth*, 24, 9, 823-828.
- 655 Jones M., Djamali M., Stevens L., Heyvaert V., Askari H., Noorollahi D., Weeks L., 2013. Mid-
656 Holocene environmental and climatic change in Iran, In book: *Ancient Iran and its neighbours:*
657 *Local developments and long-range interactions in the 4th Millennium BC.*, Edition: British
658 Institute for Persian Studies Series, Chapter: 1, Publisher: Oxbow books, Editors: Petrie C.A.
- 659 Kelts K. and Shahrabi M., 1986. Holocene sedimentology of hypersaline lake Urmia, NW Iran,
660 *Palaeogeogr., Palaeoclim., Palaeoecol.*, 54, 105-130.
- 661 Kong T., Tudryn A., Gibert-Brunet E., Motavalli-Anbaran S-H., Tucholka P., Lankarani M.,
662 Ahmady-Birgani H., Noret A., Massault M., Miska S., Late Quaternary climate and environment
663 reconstruction of Lake Urmia basin (Iran), Inqua Congress, Dublin 25-31 July 2019, Dublin,
664 Ireland.
- 665 Kuzucuoglu C., Christol A., Mouralis D., Dog A.F., Akköprü E., Fort M., Brunstein D., Zorer
666 H., Fontugne M., Karabiyikog M., Scaillet S., Reyss J.L., Guillou H., 2010. Formation of the
667 Upper Pleistocene terraces of Lake Van (Turkey), *Journal of Quaternary Science*, 25(7) 1124–
668 1137.
- 669 MacDonald G.M., Beukens R. P., Kieser W. E., 1991. Radiocarbon Dating of Limnic Sediments:
670 A Comparative Analysis and Discussion, *Ecology*, 72, 3, 1150-1155.

- 671 Neretin L., Böttcher M.L., Jorgensen B.B., Volkov I.I., Lüschen H., Hilgenfeldt K., 2004.
672 Pyritization processes and greigite formation in the advancing sulfidization front in the upper
673 Pleistocene sediments of the Black Sea, *Geochimica et Cosmochimica Acta*, 68, 9, 2081-2093.
- 674 Pengra B., 2012. The drying of Iran's lake Urmia and its environmental consequences, UNEP
675 Global Environment Alert Service (GEAS).
- 676 Reimer PJ, Bard E, Bayliss A, Beck JW, Blackwell PG, Bronk Ramsey C, Buck CE, Cheng H,
677 Edwards RL, Friedrich M, Grootes PM, Guilderson TP, Haflidason H, Hajdas I, Hatté C, Heaton
678 TJ, Hogg AG, Hughen KA, Kaiser KF, Kromer B, Manning SW, Niu M, Reimer RW, Richards
679 DA, Scott EM, Southon JR, Turney CSM, van der Plicht J., 2013. IntCal13 and MARINE13
680 radiocarbon age calibration curves 0-50000 years cal BP. *Radiocarbon* 55(4). DOI:
681 10.2458/azu_js_rc.55.16947.
- 682 Schneider L., Pain C.F., Haberle S., Blong R., Alloway B.V., Fallon S.J., Hope G., Zawadzki A.,
683 Heijnis H., 2019. Evaluating the Radiocarbon Reservoir Effect in Lake Kutubu, Papua New
684 Guinea, *Radiocarbon*, 61, 1, 287-308.
- 685 Shah-Hosseini M., (2003). Sedimentology of hypersaline Lake Urmia in central part of Shahid
686 Kalantari Highway with special reference to their origin, M.Sc. Thesis, Department of Geology,
687 University of Teheran, 98p.
- 688 Sharifi A., Pourmand A., Canuel E.A., Ferer-Tyler E., Peterson L.C., Aichner B., Feakins S.J.,
689 Daryaee T., Djamali M., Beni A.N., Lahijani H.A.K., Swart P.K., 2015. Abrupt climate
690 variability since the last deglaciation based on a high-resolution, multi-proxy peat record from
691 NW Iran: The hand that rocked the Cradle of Civilization?, *Quaternary Science Reviews*, 123,
692 215-230.
- 693 Sharifi A., Shah-Hosseini, M., Pourmand, A., Esfahaninejad, M., Haeri-Ardakani, O., 2018. The
694 Vanishing of Urmia Lake: A Geolimnological Perspective on the Hydrological Imbalance of the
695 World's Second Largest Hypersaline Lake, DOI: 10.1007/698_2018_359, *The Handbook of*
696 *Environmental Chemistry*, Springer, Berlin, Heidelberg.

- 697 Sharifi A., 2018. The Urmia Lake Environmental Crisis Man vs. Climate, The 3rd International
698 Geosciences Congress of Iran, 26/02/2018, Tehran.
- 699 Solaymani S., 2009. Evaluation de l'aléa sismique pour les villes de Téhéran, Tabriz et Zandjan
700 dans le NW de l'Iran. Approche morphotectonique et paléosismologique. Tectonique. Université
701 Montpellier 2 Sciences et Techniques du Languedoc, 2009.
- 702 Staubwasser M., Weiss H., 2006. Holocene climate and cultural evolution in late prehistoric-early
703 historic West Asia, *Quaternary Research*, 66, 372-387.
- 704 Stevens L.R., Ito E., Schwab A., Wright Jr.H.E., 2006. Timing of atmospheric precipitation in
705 the Zagros Mountains inferred from a multi-proxy record from Lake Mirabad, Iran, *Quaternary
706 research*, 66, 494-500.
- 707 Stevens L., Djamali M., Andrieu-Ponel V., de Beaulieu J., 2012. Hydroclimatic variations over
708 the last two climatic cycles at Lake Urmia, Iran. *J. of Paleolimnology* 47, 645-660.
- 709 Strehle C., André F., Jelinowska A., Tucholka P., Guichard F., Lericolais G., and Panin N.,
710 2002. Magnetic mineral as indicators of major environmental change in Holocene Black sea
711 sediments: preliminary results, *Phys.Chem. Earth*, 27, 1363-1370.
- 712 Talebi T. Ramezani E., Djamali M., Lahijani H.A.K., Naqinezhad A., Alizadeh K., Andrieu-
713 Ponel V., 2015. The Late-Holocene climate change, vegetation dynamics, lake-level changes and
714 anthropogenic impacts in the Lake Urmia region, NW Iran, *Quaternary International*,
715 <http://dx.doi.org/10.1016/j.quaint.2015.11.070>.
- 716 Tudryn A. and Tucholka P., 2004. Magnetic monitoring of thermal alteration for natural pyrite
717 and greigite, *Acta Geoph. Polon.* 52 (4), 509-520.
- 718 Tudryn A., Tucholka P., Gibert E., Gasse F., Wie K., 2010. A late Pleistocene and Holocene
719 mineral magnetic record from sediments of Lake Aibi, Dzungaria Basin, NW China, *J. of
720 Paleolimnology*, 44,1, 109-121.
- 721 Tudryn A., Chalié F., Lavrushin Yu.A., Antipov M.P., Spiridonova E.A., Lavrushin V., Tucholka
722 P., Leroy S.A.G., 2013. Late Quaternary Caspian Sea environment: Late Khazarian and Early

723 Khvalynian transgressions from the lower reaches of the Volga River, *Quaternary International*,
724 292: 193-204.

725 Tudryn A., Giannesini P.J., Guichard F., Badaut-Trauth D., Tucholka P., Boomer I., 2014. The
726 role of iron minerals in laminae formation in Late Pleistocene sediments of the Caspian Sea,
727 *Quaternary International*, 345, 68-76.

728 Wasylikowa K., Witkowski A., Walanus A., Hutorowicz A., Alexandrowich S.W., Langner J.J.,
729 2006. Palaeolimnology of Lake Zeribar, Iran, and its climatic implications, *Quaternary Research*,
730 66, 477-493.

731

732 **Figure captions**

733

734 Fig. 1. Lake Urmia: a) location of the lake, b) lake in 1999 on the left and in 2019 on the right
 735 (after Ahmady-Birgani et al., 2020), c) lake's catchment area, hydrography and dams (after
 736 Sharifi et al. et al., 2018), red circle indicates coring area, d) simplified geological map of Lake
 737 Urmia catchment area (after Sharifi et al., 2018, completed with information from Geological
 738 Map of Iran, Sheet No 1 North-West Iran).

739

740 Fig. 2. Study area: a) location of coring - red circle (Golman coring sites are labeled as G and
 741 numbers from G1 to G7), surface- and groundwater sampling - yellow circles and line, Google
 742 Earth map (geographic coordinates for all sites are indicated on Tab. 1), b) upper picture - gas
 743 and under-pressure mud rising up along the borehole Golman 2 after coring in May 2016, lower
 744 pictures - crystallization of muddy salt on the borehole surface, September 2017, c) lake water
 745 sampling site at the foot of the east-west dike-type highway in May 2016; arrows indicate two
 746 salty lines that highlight water level change in spring 2016, d) lake water sampling site close to
 747 the coring Golman 4: above - May 2016, below - September 2017, e) sediment cores Golman 4
 748 and Golman 7 obtained from recently dried out part of the lake, optical microphotograph from
 749 core Golman 7 for: f) sand at 12.49 m depth, g) fine silty, carbonate rich sediment at 10.66 m
 750 depth, h) fecal pellet rich sediment at 3.62 m depth.

751

752 Fig. 3. Parameters measured on water (in-situ measurements) and on sediments : a) electric
 753 conductivity *versus* pH for water samples from Lake Urmia, River Shahr Chai, wells between
 754 Urmia City and the lake border, coring wells, A – captive brine rising-up from intermediated
 755 depth (below 4.5-5m), B – captive brine rising-up from the bottom of the core, b) classification of
 756 magnetic minerals in terms of magnetization and coercivity ratios after Day et al. (1977);
 757 sediments from cores Golman 5 and Golman 7: black triangles - SD magnetic grain sizes, circles

758 - PSD-like and squares - MD magnetic grain, typical magnetic hysteresis loop of bulk sediment
 759 samples with c) MD magnetic grain sizes and d) SD magnetic grain sizes, typical
 760 thermomagnetic curve of bulk sediment samples with e) magnetite and f) greigite, g) X-ray
 761 diffraction pattern obtained for magnetic extract from core Golman 5 at 2.50 m depth with mean
 762 identified minerals: greigite (Gr), which is highlighted by vertical blue lines, albite (Al), calcite
 763 (Ca), chlorite (Ch), muscovite (Mu), pyrite (Py), quartz (Qu).

764

765 Fig. 4. Down-core variation in magnetic susceptibility (black line) and carbonate contents (blue
 766 line) for cores: a) Golman 4, b) Golman 5, c) Golman 3, d) Golman 7 and e) Golman 6. Depth
 767 scale for core Golman 4 is different from common scale for others cores. Lithological log is
 768 presented for core Golman 4. ^{14}C dating for cores Golman 5 (G5), Golman 6 (G6) and Golman 7
 769 (G7) are indicated on the common depth scale and as red arrows on corresponding cores. Grey
 770 band that shows increased magnetic susceptibility through cores, and grey solid and dashed lines
 771 indicate correlations between different cores. Sequences compressed during coring are presented
 772 after linear decompression.

773

774 Fig. 5 Down-core variation in lithology and in a) magnetic susceptibility, b) magnetic mineralogy
 775 with M for magnetite (circle) and G for greigite (black triangle), c) water contents in the
 776 sediment, d) relative salinity on wet sediment samples, e) mean sediment grain size, f) carbonate
 777 contents, g) specific carbonate contents. ^{14}C cal BP dates are presented on the left of the depth
 778 scale. Lithology, a), b), c), e) and f) present composite data from cores Golman 6 and 7 while d)
 779 and g) present data from core Golman 7.

780

781

782 Tab. 1. Location of sampling sites, both water and sediment in the vicinity of Urmia City, and the
783 results of in situ measurements of pH, temperature and electric conductivity. Measurements of
784 surface water, groundwater from wells and groundwater rising-up from coring well Golman 5,
785 have been done in May 2016 or in September 2017. Measurements of groundwater rising-up
786 from coring wells Golman 1, Golman 2 and Golman 3, have been done in May 2016 and in
787 September 2017.

788

789 Tab. 2 ^{14}C AMS and $\delta^{13}\text{C}$ data for cores Golman 6 (G6), Golman 7 (G7) and Golman 5 (G5).
790 The calibrated ages are the mean ages.

791

792

793

794

795

796

797

798

799

800

801

802

803

804

805

806

807

	Site name	comment on sampling	latitude	longitude	altitude m asl ±1 m	pH	temp. °C	conduct. mS.cm ⁻¹
river SHAHR CHAI	BARDESOOR	above dam, near Silvana City, 09/2017	37°26'14.592"	44°49'26.92"	1606	8.38	13.8	0.299
	SHAH 1	Urmia City, 05/2016	37°31'35.24"	45°02'50.53"	1354	8.41	14.2	0.249
	SHAH 2	between Urmia City and the river outlet, 05/2016	37°33'16.93"	45°16'12.26"	1276	7.83	16.9	3.40
well	SALEH ABAD	in "Amir's garden", 09/2017	37°31'16.626"	45°10'52.812"	1294	7.28	14.2	0.884
	KESH 1	Kesh Tiban, 09/2017	37°32'28.788"	45°14'07.224"	1281	8.13	19.9	0.575
	GOLMAN 0	close to GOLMAN coring site, 05/2016	37°35'15.44"	45°15'19.70"	1278	7.35	15.3	1.18
	HAJILAR 1	1st after sampling SHAH 2, 05/2016	37°33'22.00"	45°16'17.51"	1277	6.29	15.4	3.12
	HAJILAR 2a	Double well - large well, 05/2016	37°33'09.07"	45°16'08.95"	1276	6.12	15.1	12.22
	HAJILAR 2b	Double well - small well, 05/2016	37°33'09.07"	45°16'08.95"	1276	6.63	16.2	12.39
coring well	GOLMAN 1	9 m deep, 05/2016	37°35'35.86"	45°16'26.77"	1270	6.84	29.6	222.0
	GOLMAN 1	9 m deep, 09/2017	37°35'35.86"	45°16'26.77"	1270	6.05	30.1	227.0
	GOLMAN 2	14 m deep, 05/2016	37°35'35.09"	45°16'28.60"	1270	5.80	29.2	219.0
	GOLMAN 2	14 m deep, 09/2017	37°35'35.09"	45°16'28.60"	1270	5.80	31.8	217.0
	GOLMAN 5	5.25 m deep, 09/2017	37°35'33.4"	45°16'27.6"	1270	6.04	26.6	222.0
	GOLMAN 3	14.2 m deep, pressurized water, 05/2016	37°35'33.09"	45°16'31.20"	1270	6.48	25.0	141.1
	GOLMAN 3	14.2 m deep, inside coring tubing, 05/2016	37°35'33.09"	45°16'31.20"	1270	6.35	20.2	147.1
	GOLMAN 3	14.2 m deep, inside coring tubing, 09/2017	37°35'33.09"	45°16'31.20"	1270	6.24	18.9	142.0
	GOLMAN 3	14.2 m deep, outside tubing, 05/2016	37°35'33.09"	45°16'31.20"	1270	6.61	27.5	158.8
	GOLMAN 3	14.2 m deep, outside tubing, 09/2017	37°35'33.09"	45°16'31.20"	1270	6.29	19.1	140.0
	GOLMAN 4	0.6 m deep	37°35'37.31"	45°16'38.38"	1270			
	GOLMAN 6	8 m deep	37°35'28.854"	45°16'33.834"	1270			
	GOLMAN 7	12.5 m deep, pressurized water	37°35'28.746"	45°16'33.75"	1270			
lake	GOLMAN	near coring GOLMAN 4, 05/2016	37°35'37.31"	45°16'38.38"	1270	8.02	21.3	207.0

	Dam-bridge1	N side of the causeway, 05/2016	37°46'31.62"	45°19'47.04"	1270	7.53	27.9	190.2
810	tap water	Urmia city	05/2016					0.323

811 Table 2

812

813

814	Core	Sample	Depth	Analyze Nr	Nature	¹⁴ C Age		Cal ¹⁴ C Age		 ¹³ C
815			(m)			(yr BP)	(yr)	(cal yr BP) ^(*)	(yr)	(‰ PDB)
816										
817	G6	G6-4.40	4.40	I2553/B2304	OM	17561	76	21 200	210	-24.20
818										
819	G7	G7-S2 2.80	2.80	I2218/B2097	Charcoal	4 734	22	5 520	100	-26.50/-13.50
820		G7-S3 4.05	4.05	I2525/B2297	OM	15 088	66	18 340	190	-25.30
821		G7-S8 12.46	12.46	I2524/B2301	Charcoal	25 591	96	29 700	360	-24.60
822										
823	G5	G5 2.34	2.34	I2141/B2087	Charcoal	4 343	25	4 900	60	-14.50
824		G5 3.66	2.66	I2142/B2088	Charcoal	4 394	22	4 950	65	-25.50

825

826 ^(*) Reimer et al, 2013. IntCal13 and MARINE13 radiocarbon age calibration curves 0-50000 years cal BP. *Radiocarbon*, 55(4). DOI:
827 10.2458/azu_js_rc.55.16947

828

829

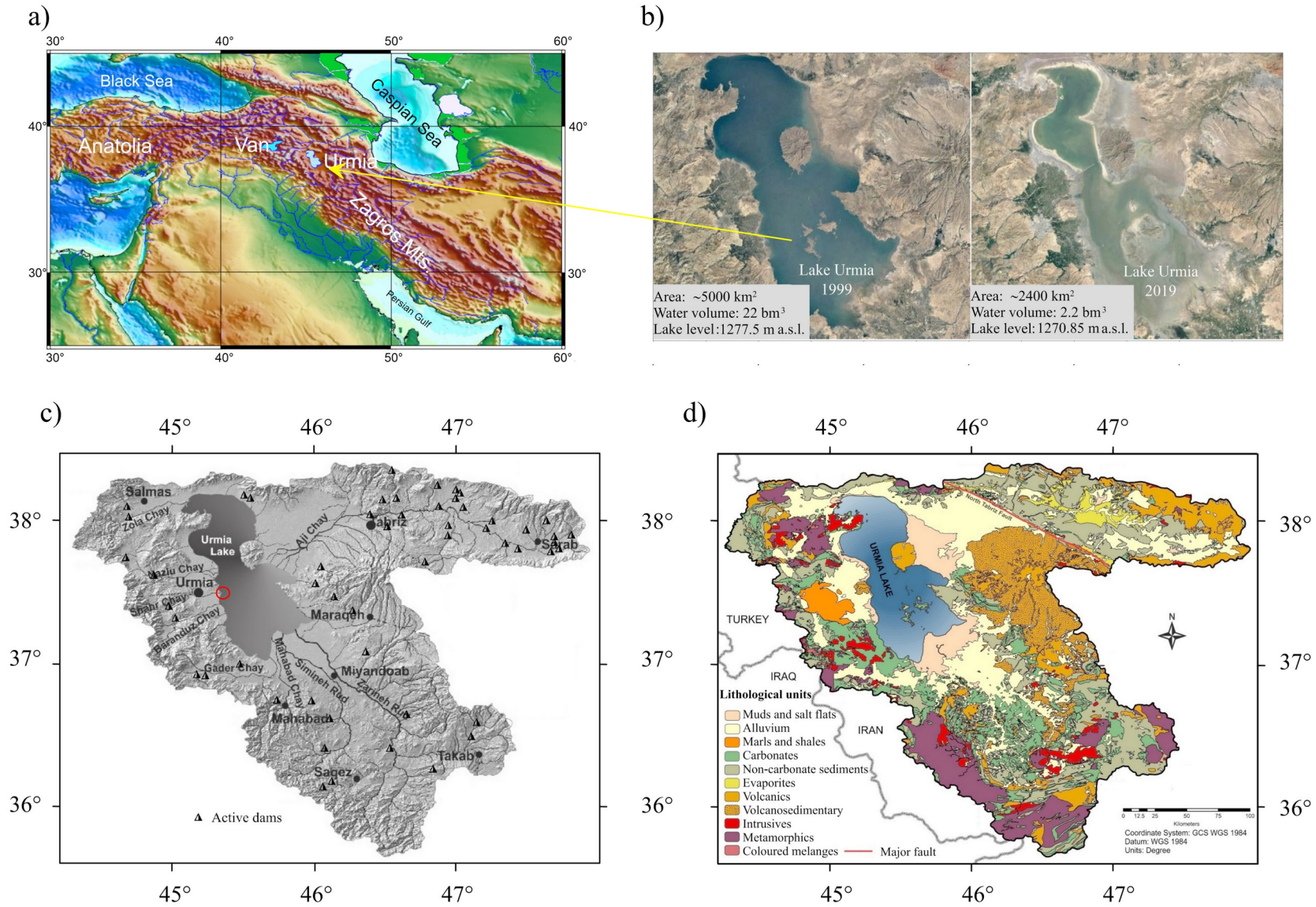
830

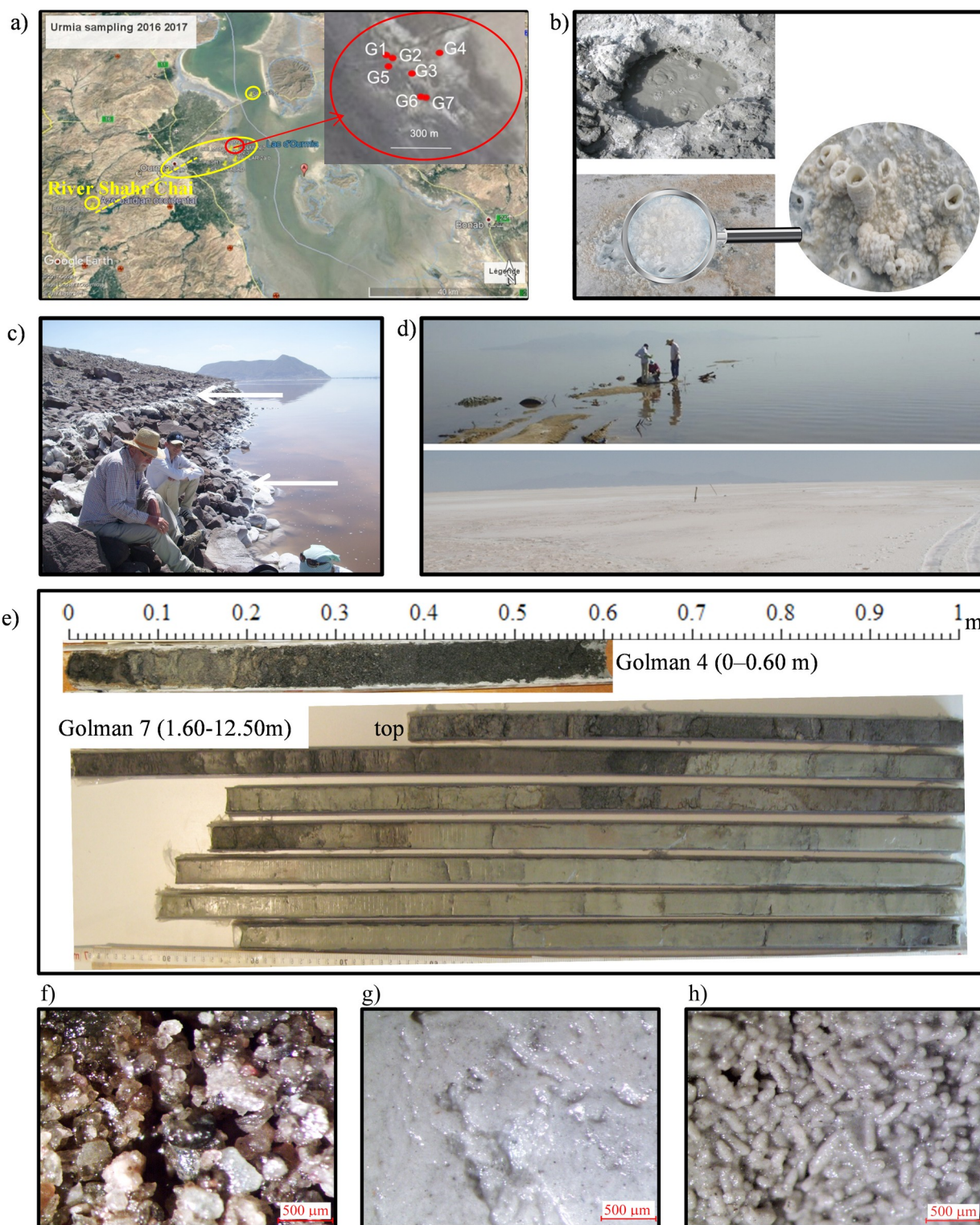
831

832

833

834 Figure 1





837

838

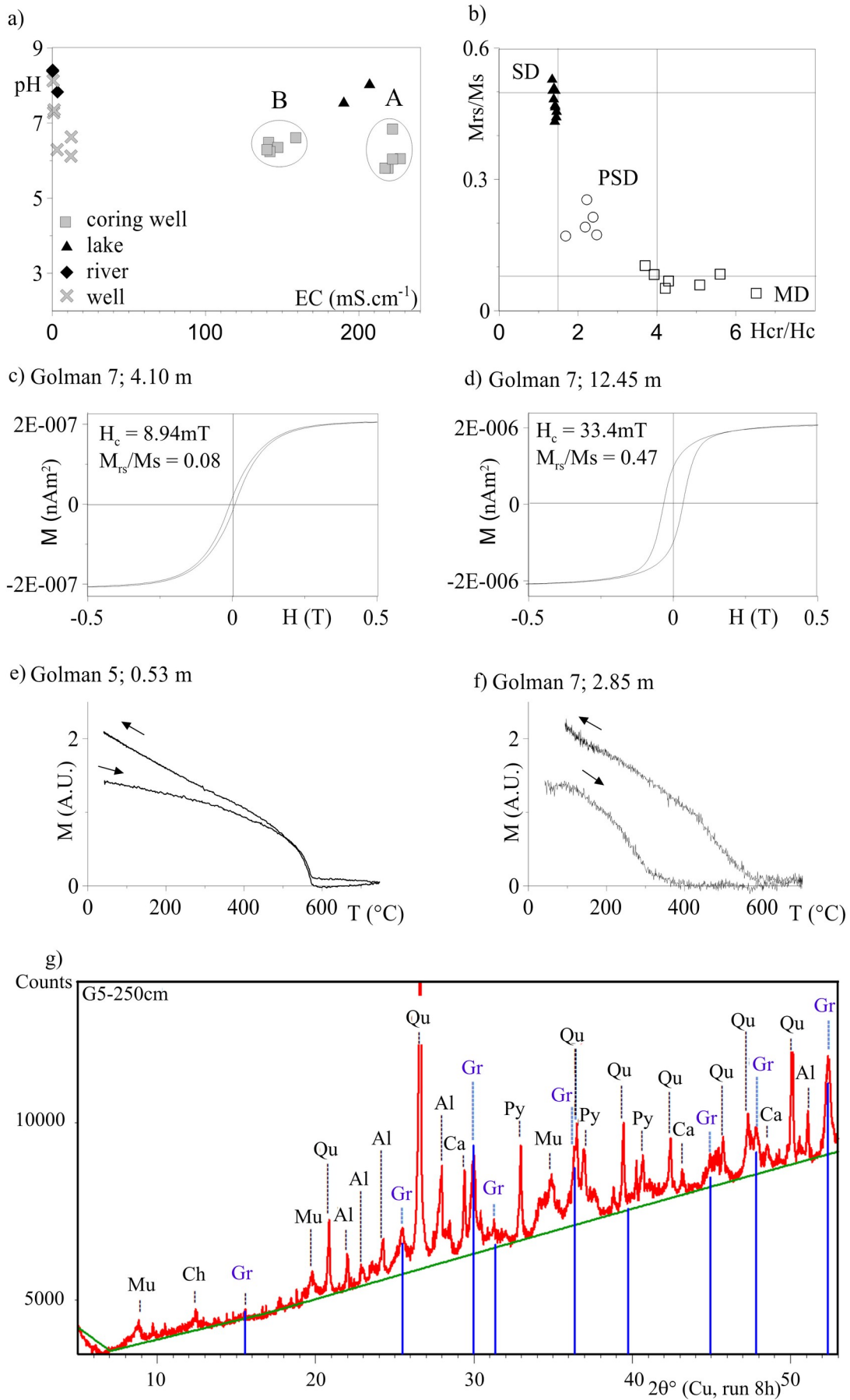
839

840

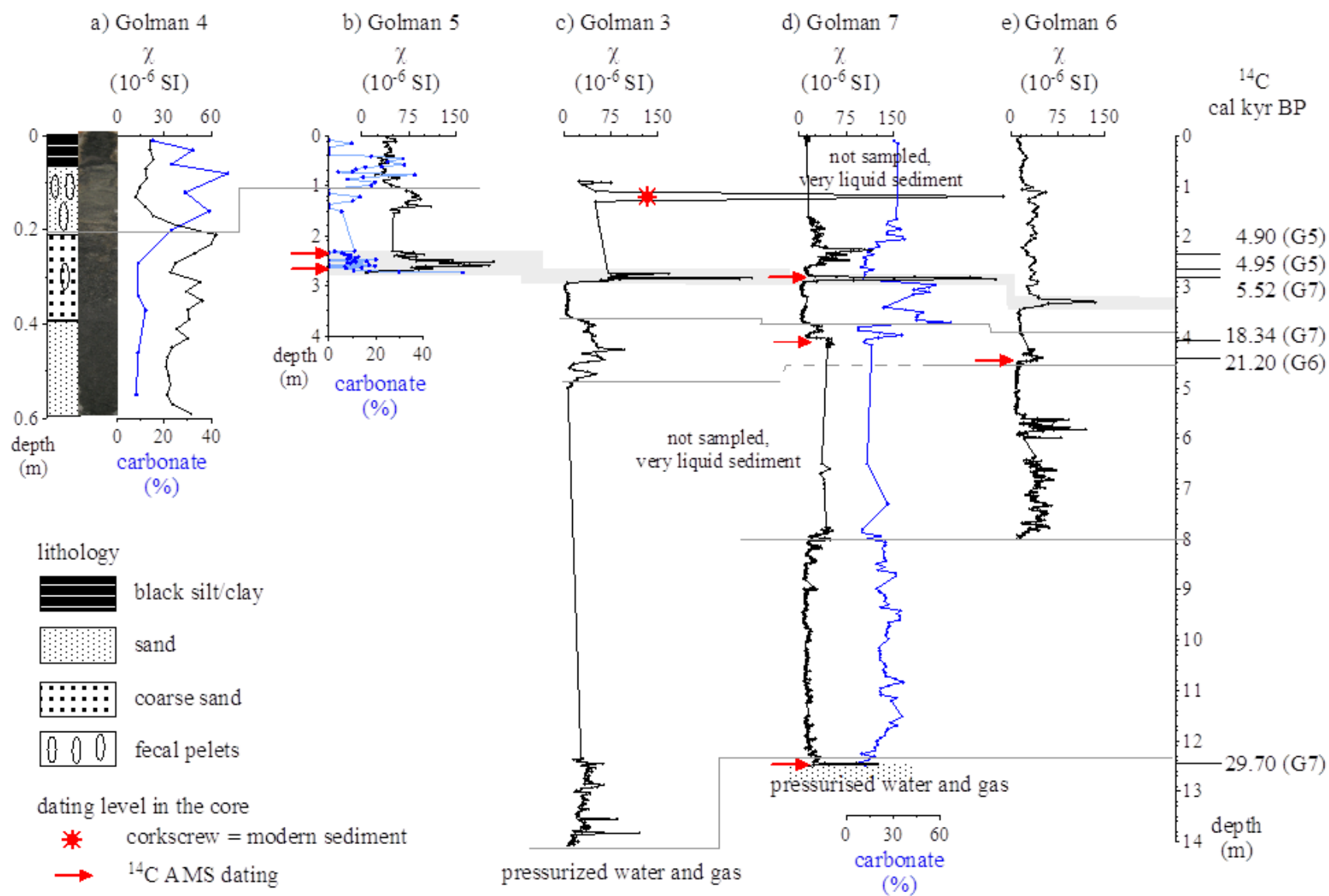
841

842

843 Figure 3



845 Figure 4



847 Figure 5

